UNIVERSITÄT AUGSBURG
Universitätsbibliothek

OPEN ACCESS
OPUS AUGSBURG

Spatiotemporal dynamics and multi-scale diagnosis of urban resilience to typhoon disaster chains in Fujian, China

Xiaoliu Yang, Laiyin Zhu, Xiaochen Qin, Xiang Zhou, Miaomiao Ma, Ying Chen, Jianhui Wei, Lu Gao, Harald Kunstmann

Angaben zur Veröffentlichung / Publication details:

Yang, Xiaoliu, Laiyin Zhu, Xiaochen Qin, Xiang Zhou, Miaomiao Ma, Ying Chen, Jianhui Wei, Lu Gao, and Harald Kunstmann. 2026. "Spatiotemporal dynamics and multi-scale diagnosis of urban resilience to typhoon disaster chains in Fujian, China." *International Journal of Disaster Risk Science*. https://doi.org/10.1007/s13753-026-00763-5.

Nutzungsbedingungen / Terms of use:

CC BY 4.0

Dieses Dokument wird unter folgenden Bedingungen zur Verfügung gestellt: / This document is made available under these conditions:
CC-BY 4.0: Creative Commons: Namensnennung
Weitere Informationen finden Sie unter: / For more information see:
https://creativecommons.org/licenses/by/4.0/deed.de

International Journal of Disaster Risk Science
https://doi.org/10.1007/s13753-026-00763-5

www.ijdrs.com
www.springer.com/13753

ARTICLE

Spatiotemporal Dynamics and Multi-Scale Diagnosis of Urban Resilience to Typhoon Disaster Chains in Fujian, China

Xiaoliu Yang[1] · Laiyin Zhu[2] · Xiaochen Qin[3] · Xiang Zhou[4] · Miaomiao Ma[5] · Ying Chen[1,6,7] · Jianhui Wei[8] · Lu Gao[1,6,7] · Harald Kunstmann[8,9,10]

Received: 1 February 2026 / Accepted: 21 August 2026
© The Author(s) 2026

Abstract

Coastal cities in southeastern China face increasing threats from typhoon-induced compound disasters (for example, torrential rainfall, urban waterlogging, and storm surges) that can cascade into interconnected disaster chains under climate change and rapid urbanization. However, dynamic multi-scale assessments of resilience to such compound disasters remain limited. This study develops an integrated framework that combines multi-scale geospatial analysis with explainable machine learning (XGBoost-SHAP). Using Fujian Province as a case study, we assess typhoon disaster chain urban resilience (TDCUR) in 2010, 2015, and 2020 across grid, administrative unit, and watershed scales, characterize spatiotemporal patterns, and apply XGBoost-SHAP as a post hoc diagnostic to summarize nonlinear indicator-TDCUR association patterns and their spatial concentration under the predefined TDCUR framework. The results indicate that: (1) Provincial TDCUR increased by 6.9% and regional disparities converged, yet major coastal cities experienced declining resilience despite strong economic development; (2) Resilience showed pronounced spatial polarization, with low-resilience cold spots expanding by 48% and clustering in the Xiamen-Quanzhou area; (3) Machine learning diagnostics indicate that typhoon-strong wind-storm surge sensitivity (B8), typhoon-rainfall-flood sensitivity (B7), and impervious surface proportion (A2) show the strongest model-based associations with the spatial variation of TDCUR and display significant interaction effects; and (4) SHAP-based spatial diagnosis identifies the Xiamen-Quanzhou-Fuzhou coastal belt and the Jinjiang Basin as priority areas with concentrated low TDCUR and high cumulative SHAP magnitudes. The proposed framework is transferable and can support spatial screening for targeted resilience actions in coastal regions, with implications for SDG 11.

Keywords Fujian · Multi-scale assessment · SHapley additive exPlanations · Typhoon disaster chains · Urban resilience

✉ Lu Gao
l.gao@foxmail.com

1 School of Geographical Sciences, Fujian Normal University, Fuzhou 350117, China

2 School of Environment, Geography, and Sustainability, Western Michigan University, Kalamazoo, MI 49008, USA

3 Faculty of Geographical Science, Beijing Normal University, Beijing 100875, China

4 Disaster Reduction Center of Fujian Province, Fuzhou 350001, China

5 China Institute of Water Resources and Hydropower Research, Beijing 100038, China

6 Key Laboratory for Humid Subtropical Eco-Geographical Processes of the Ministry of Education, Fujian Normal University, Fuzhou 350117, China

7 Fujian Provincial Engineering Research Center for Monitoring and Accessing Terrestrial Disasters, Fujian Normal University, Fuzhou 350117, China

8 Institute of Meteorology and Climate Research (IMKIFU), Karlsruhe Institute of Technology, Campus Alpin, 82467 Garmisch-Partenkirchen, Germany

9 Institute of Geography, University of Augsburg, 86159 Augsburg, Germany

10 Centre for Climate Resilience, University of Augsburg, 86159 Augsburg, Germany

Published online: 28 August 2026

1 Introduction

Under the intertwined pressures of global climate change and rapid urbanization, coastal cities are confronting increasingly severe threats from typhoon disaster chains. As intense tropical cyclones originating in the northwestern Pacific, typhoons are often accompanied by strong winds, torrential rainfall, and storm surges, triggering secondary disasters such as flooding and urban waterlogging. These processes together form a compound disaster chain system characterized by multi-hazard coupling and cross-scale propagation (Gori et al. 2022; Chen et al. 2024; Li et al. 2025; Qin et al. 2025). Such disaster chains can generate widespread impacts and amplify losses, increasing urban vulnerability and complicating conventional single-hazard risk assessments (Zscheischler et al. 2018; Ranjan and Karmakar 2024; Yang et al. 2025). Although uncertainties remain regarding future typhoon frequency, intensity-related metrics—such as maximum wind speed and rainfall intensity—are projected to increase, potentially elevating the likelihood of concurrent extreme precipitation and storm surges (Knutson et al. 2010; Bevacqua et al. 2020). In this context, conventional single-hazard, single-scale assessment and governance approaches are increasingly inadequate for addressing the systemic challenges posed by typhoon disaster chains, highlighting the need for integrated frameworks that account for compound risks and multi-level decision making.

In response to compound disaster risks, resilience—defined as a system's capacity to withstand shocks, adapt to change, and achieve sustainable recovery—has emerged as a key concept in urban disaster risk management and spatial planning (Folke 2006; UNISDR 2009; Zhang et al. 2025). In the urban context, resilience refers to a city's ability to reduce losses, maintain essential functions, adapt under changing conditions, and support recovery and sustainable development when facing expected or sudden shocks (Amirzadeh et al. 2022; Davtalab and Byčenkienė 2026). This concept has gained global recognition since the early twenty-first century, supported by initiatives such as UNISDR's 2011 report "Making Our Cities More Resilient" and the Rockefeller Foundation's 2013 "100 Resilient Cities Worldwide" project, which have promoted the integration of resilience objectives into urban planning. China has also elevated "building resilient cities" as a national priority in its 14th Five-Year Plan, with related practices implemented in major cities including Beijing, Shanghai, and Guangzhou (Lin, He, et al. 2022; Lin, Peng, et al. 2022; Mu et al. 2022; Wu et al. 2025).

As the resilience concept transitions from theory to practice, establishing scientifically sound evaluation systems has become crucial for advancing resilience building. Academic research has progressively developed indicator-based quantitative assessment methods, using multi-dimensional frameworks to characterize urban resilience and provide decision support for adaptive governance (Liu et al. 2019; Zhang et al. 2025; Xi et al. 2026). Recent studies have further incorporated a full disaster-cycle perspective—pre-, during, and post-event—into assessment systems, with applications across spatial, social, and infrastructural domains in cities such as Tokyo, Toronto, and Wuhan (Mohtat and Khirfan 2022; Liang et al. 2024; Kou et al. 2025). Within specific hazard contexts, however, existing research still largely focuses on single hazards or single disaster chains. In pluvial-fluvial flooding studies, urban resilience is often found to improve over time with narrowing regional disparities, while communities with higher socioeconomic status tend to exhibit greater flood resilience (Laurien et al. 2020; Liang et al. 2024). However, some cities have experienced declines in absorptive and adaptive capacities (Xie et al. 2023). Climate-scenario assessments further suggest that urban flood resilience may deteriorate under future climate conditions. For instance, assessments based on the Pressure-State-Response model indicate that Guangzhou's flood resilience, although currently moderate and slowly improving, may decline under multiple Representative Concentration Pathway scenarios during 2050–2070 (Ruan et al. 2021).

Although existing research provides a foundation for understanding urban resilience, three critical limitations persist in addressing typhoon disaster chains as complex systems: First, most studies focus on single disasters or single disaster chains, and therefore do not adequately capture multi-chain, concurrent disaster effects triggered by typhoons—a limitation that is particularly evident in topographically complex, densely populated coastal mountainous cities. Second, assessment scales are often confined to a single administrative unit, with limited analysis of cross-scale linkages from inland to coastal areas and from upstream to downstream regions, which constrains differentiated decision making across provincial, municipal, and county governance levels. Third, conventional statistical approaches often have difficulty representing complex nonlinear relationships and identifying critical thresholds in resilience-related mechanisms, creating a gap between mechanistic understanding and actionable governance practice.

To address these gaps, this study develops an interpretable, multi-scale assessment framework for urban resilience to typhoon disaster chains, using Fujian Province, China, as a case study. The framework evaluates typhoon disaster chain urban resilience (TDCUR) on 30-arc-second (~1 km) grids for 2010, 2015, and 2020 and then aggregates results to county, city, and basin scales to support cross-level governance. Indicator weights for index aggregation are pre-specified using an objective procedure that integrates

GeoDetector-based spatial stratified heterogeneity (q-statistics) and recursive entropy weights, followed by linear fusion and normalization to obtain the final fused weight vector. Building on the predefined TDCUR formulation, we apply XGBoost with SHapley Additive exPlanations (SHAP) strictly as a post hoc diagnostic tool. This analysis is used to characterize nonlinear association patterns, interaction structures, and spatial heterogeneity, and to identify areas where multiple indicators jointly show strong model-based associations with low TDCUR. Accordingly, this study aims to: (1) establish a dynamic, multi-scale assessment methodology for resilience to typhoon disaster chains; (2) reveal spatiotemporal evolution and regional differentiation of TDCUR across scales; (3) diagnose dominant nonlinear associations, interactions, and empirical turning points (that is, data-driven change points in model responses) under the predefined formulation; and (4) provide spatial decision-support evidence for prioritizing resilience enhancement in coastal mountainous cities and advancing SDG 11.

2 Materials and Methods

This section describes the study area and urban delineation and summarizes the data sources. It then presents the TDCUR assessment approach, including the indicator system, objective weight specification and index computation with uncertainty assessment, multi-scale aggregation, spatiotemporal pattern analysis (KDE and hotspot analysis), and a post hoc XGBoost-SHAP diagnostic analysis. Additional details are provided in the Supplementary Information.[1]

2.1 Study Area

Fujian Province (23°33'–28°20'N, 115°50'–120°40'E) is located on the southeastern coast of China and lies within a region frequently affected by typhoon landfalls. It has a coastline of approximately 3,324 km and constitutes one of East Asia's most vulnerable land-sea interface zones under the influence of the East Asian monsoon. Administratively, the province comprises nine prefecture-level cities and 84 county-level divisions, including the Pingtan Comprehensive Experimental Zone. As shown in Fig. 1, the study area covers eight major river-basin units, including the Minjiang Basin, inland single-inflow combined basins (LS), and coastal single-inflow combined basins (CS). Its complex topography and distinctive geographic setting contribute to diverse typhoon-induced disaster chains. Based on official statistics for 2000–2020, typhoon events caused an average annual direct economic loss of approximately CNY 12.74 billion, accounting for 58.3% (95% CI: 51.5%–65.1%) of total natural hazard-related losses in Fujian. Notably, compound typhoon disaster chains contributed more than 76% of typhoon-associated losses (Huang et al. 2022; Tian et al. 2023).

In this study, urban areas in Fujian Province are delineated using the 2020 population density dataset, defined as contiguous tracts with a population density of at least 600 persons/km^2, consistent with approaches applied in previous studies (Pesaresi et al. 2013; Li and Qiu 2015). The total delineated urban extent covers approximately 9,680.6 km^2 (Fig. 1c). All subsequent analyses of typhoon disaster chain urban resilience (TDCUR) were conducted specifically within these defined urban boundaries.

2.2 Data Sources

This study integrates data of three primary categories (Table 1). The first category comprises baseline geographic data layers, including administrative boundaries at the provincial, municipal, and county levels, coastline delineations, and major river basin polygons. The second category includes socioeconomic data derived from official surveys, specifically county-level economic statistics, urban infrastructure inventories, and population census records. The third category consists of remote sensing and GIS products in raster and vector formats—namely land cover maps, a digital elevation model (DEM), and vector-based road and river network layers. All datasets were resampled using bilinear interpolation and harmonized to a consistent 30-arc-second (approximately 1 km) spatial resolution grid to ensure geographic and analytical consistency.

2.3 Conceptual Framework for Typhoon Disaster Chain Urban Resilience (TDCUR)

We propose a three-component framework to assess TDCUR within Fujian's urban areas (population density ≥ 600 persons/km^2). First, TDCUR is organized into three capacity dimensions—absorption, coping, and recovery and adaptation—and operationalized using a 21-indicator system capturing terrain, infrastructure, and socioeconomic conditions. Second, indicators are analyzed on a 30-arc-second (~1 km) grid and aggregated to county, city, and basin units. Indicator weights are specified a priori using an objective procedure that combines q-statistic-based spatial stratified heterogeneity with recursive entropy weights through linear fusion, followed by normalization. We compute grid-level indices with Monte Carlo-based weight perturbation uncertainty, and characterize spatiotemporal patterns using kernel density estimation and Getis-Ord Gi* hotspot analysis. To ensure strict interannual comparability, all year-to-year

[1] https://pan.quark.cn/list#/doc/255a19c7167140d1bab8f40d9ec79254

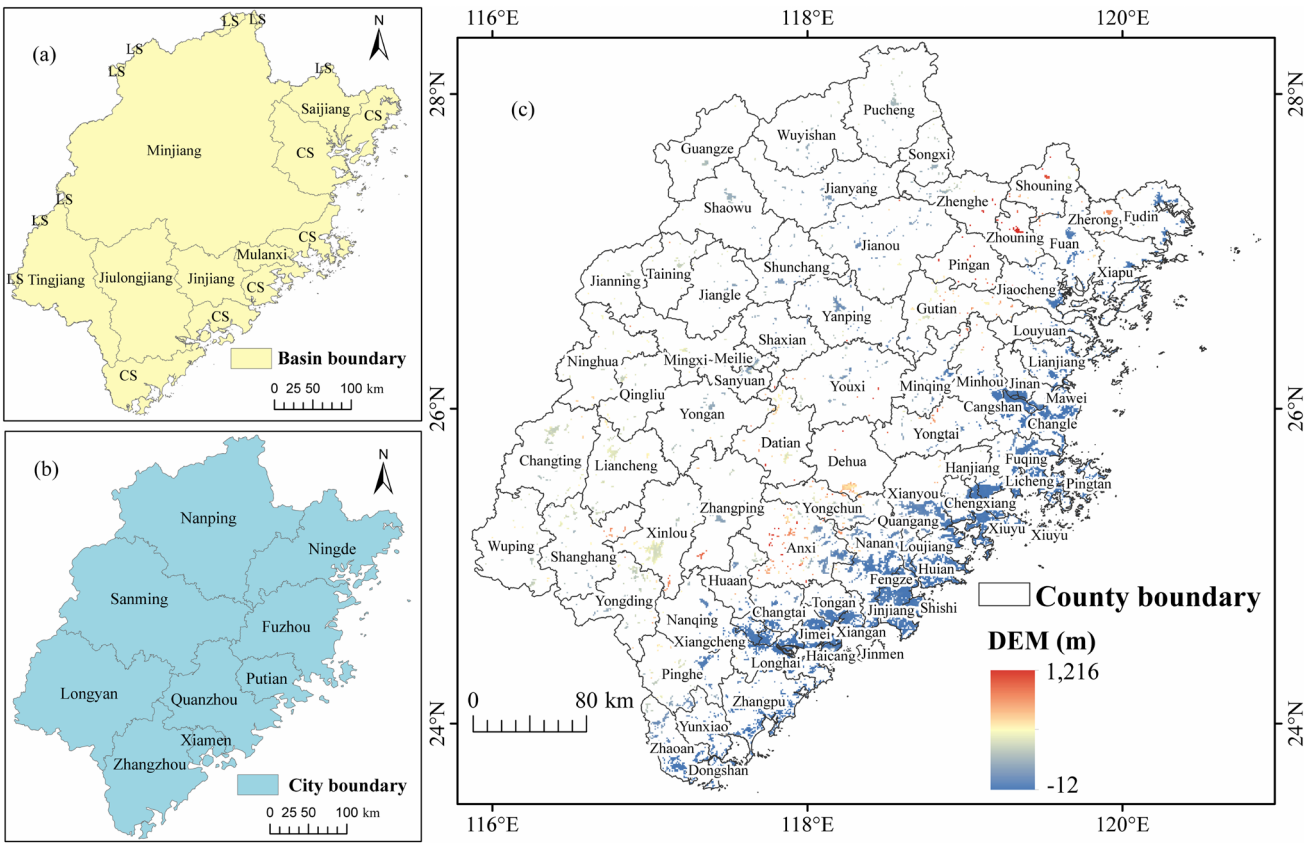


Fig. 1 Study area in Fujian Province, China. **a** River-basin units (LS: inland single-inflow combined basins; CS: coastal single-inflow combined basins); **b** Prefecture-level cities; **c** Counties and DEM-derived elevation within the delineated urban analysis domain; white areas denote locations outside this domain

analyses (2010, 2015, 2020) are conducted within a fixed urban mask defined by the 2020 urban extent. Third, we apply XGBoost-SHAP strictly as a post hoc diagnostic layer to characterize nonlinear association patterns, interactions, and spatial heterogeneity under the predefined TDCUR formulation. Multi-scale Σ|SHAP| summaries are used to identify areas where multiple indicators jointly show strong model-based associations with low TDCUR, providing diagnostic evidence to support spatial prioritization (Fig.2).

2.4 Construction of the Evaluation Indicator System

This study evaluates TDCUR across three compound disaster sequences: Typhoon-Rainstorm-Urban Waterlogging (TRU), Typhoon-Rainstorm-Flooding (TRF), and Typhoon-Strong Wind-Storm Surge (TWS). These sequences guide indicator construction and interpretation and are represented by chain-sensitivity indicators in the coping dimension (B3 for TRU, B7 for TRF, and B8 for TWS; Table 2 and Supplementary S1[1]). Resilience is conceptualized as the capacity to withstand shocks, manage impacts, and recover and adapt over time (Yu et al. 2023; Liang et al. 2024). Indicators are organized into three components—absorption, coping, and recovery and adaptation—comprising 21 indicators in total (A1–A6, B1–B8, C1–C7; Table 2). Notably, B3, B7, and B8 are independently derived proxy indices of chain-specific disaster-forming environment sensitivity and are incorporated as adverse coping-related conditions (that is, higher values indicate greater sensitivity and thus lower coping capacity), rather than being re-estimated from the TDCUR aggregation formula. Detailed indicator definitions and measurement methods are provided in Table 2; Supplementary S1[1] documents the derivation of B3, B7, and B8; and Supplementary S4[1] provides additional indicator interpretations.

2.5 Quantifying Typhoon Disaster Chain Urban Resilience (TDCUR)

Typhoon disaster chain urban resilience is computed as a linear weighted aggregation of min-max normalized indicators. Indicator weights are specified a priori using an objective procedure that combines q-statistic-based spatial stratified heterogeneity and recursive entropy weights via linear fusion

Table 1 Datasets and variables used in this study

Type	Dataset	Resolution	Period	Source
Baseline geographic layers	Administrative division data	–	2024	Tianditu (http://lbs.tianditu.gov.cn/home.html)
	Coastline data	–	2020	Global Self-consistent, Hierarchical, High-resolution Geography (GSHHG) Database (https://www.ngdc.noaa.gov/mgg/shorelines/shorelines.html)
	Basin boundary data	–	2020	Fujian Provincial Department of Water Resources
Socioeconomic survey data	Population and GDP data	1 km	2010, 2015, and 2020	Data Center for Resources and Environmental Sciences (https://www.resdc.cn/)
	Healthcare and shelter data	County	2020	Fujian Provincial Emergency Department and Fujian Disaster Reduction Center
Remote-sensing/GIS products	Digital elevation model (DEM)	30 m	2020	Data Center for Resources and Environmental Sciences (https://www.resdc.cn/)
	Land use and land cover (LULC)	30 m	2010, 2015, and 2020	Data Center for Resources and Environmental Sciences (https://www.resdc.cn/)
	Road network data	–	2010, 2015, and 2020	OpenStreetMap Data (https://www.openstreetmap.org)
	Difference Vegetation Index	30 m	2010, 2015, and 2020	Data Center for Resources and Environmental Sciences (https://www.resdc.cn/)
	Impervious surface data	30 m	2010, 2015, and 2020	International Research Center of Big Data for Sustainable Development Goals (CBAS)
	Open space data	–	2020	Geographic Data Sharing Infrastructure, global resources data cloud (www.gis5g.com)

and normalization. In the main text, we present the population-aware multi-scale aggregation method (Sect. 2.5.1) and the XGBoost-SHAP-based post hoc diagnostic analysis (Sect. 2.5.2). Detailed derivations and implementation settings for weight construction (including the fusion/normalization procedure) and Monte Carlo weight perturbation uncertainty assessment are provided in Supplementary Methods (S4[1]).

2.5.1 Multi-scale Aggregation of Resilience

To translate grid-level resilience results into decision-relevant spatial units, TDCUR values are aggregated from 30-arc-second grids to county, city, and basin scales using a population-aware aggregation approach that accounts for exposure and spatial heterogeneity (Wang et al. 2024; Yang et al. 2025).

Step 1: Effective exposure weight. For each grid cell i, exposed population is calculated as:

$$pop_i = A_i \times P_i, \tag{1}$$

where A_i denotes the grid-cell area and P_i population density. To emphasize grid cells characterized by high exposure and relatively low baseline resilience, an effective exposure weight is defined as:

$$w_i^{eff} = pop_i \exp(-\lambda H_i),\ H_i = -R_i \ln(R_i + \varepsilon), \tag{2}$$

where R_i denotes the baseline grid-level TDCUR value,λ is an entropy-based penalty coefficient controlling the strength of resilience adjustment, and ε is a small numerical guard to avoid logarithmic instability. This formulation ensures that grid cells with lower resilience receive relatively higher effective weights, while high-resilience cells are progressively down-weighted. The value of λ was set to 0.7 to provide moderate penalization of high-resilience grid cells; sensitivity tests indicate that reasonable variations in λ do not alter the overall spatial pattern.

Step 2: Within-unit aggregation. For a target spatial unit U(county, city, or basin), the exposure-adjusted resilience index is calculated as:

$$TDCUR_U = \frac{\sum_{i \in U} w_i^{eff} R_i}{\sum_{i \in U} w_i^{eff}}. \tag{3}$$

Step 3: population emphasis. While Step 2 integrates exposure and resilience at the grid level, Step 3 summarizes the internal population exposure structure of each

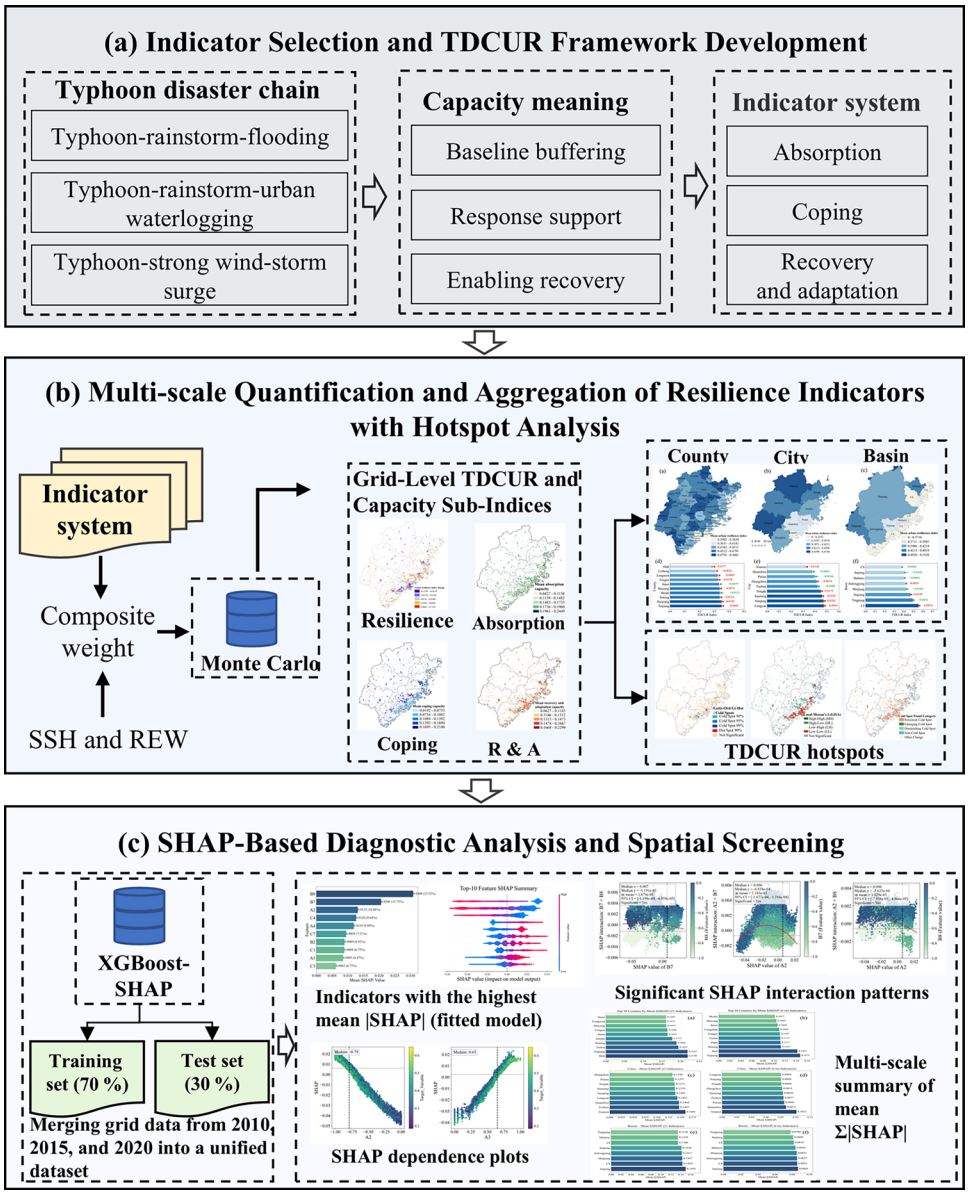


Fig. 2 Design and framework of the study. TDCUR = Typhoon disaster chain urban resilience, SSH = Spatial stratified heterogeneity, REW = Recursive entropy weights, R & A = Recovery and adaptation, SHAP = SHapley Additive exPlanations

spatial unit. The proportion of exposed population is calculated as:

$$S_U = \frac{\sum_{i \in U} pop_i}{P_U}, \tag{4}$$

where P_U denotes the census population of unit U. The final multi-scale resilience index is defined as:

$$TDCUR_U^* = TDCUR_U \times S_U. \tag{5}$$

2.5.2 XGBoost-SHapley Additive exPlanations (SHAP)-Based Diagnostic Analysis

To characterize spatial heterogeneity, nonlinear indicator-TDCUR associations, and interaction patterns under the predefined TDCUR framework, XGBoost regression is combined with SHAP-based interpretation methods (Alam et al. 2020; Zyl et al. 2024; Yin et al. 2025). The analysis is implemented as a post hoc diagnostic, and SHAP values are interpreted as model-based associations and interaction patterns.

Step 1: Data preparation. Grid-level observations from 2010, 2015, and 2020 are combined into a unified dataset. The 21 indicators constitute the feature matrix X, and the mean grid-level TDCUR estimates from the Monte Carlo

Table 2 Indicators for assessing typhoon disaster chain urban resilience (TDCUR)

Resilience	Code	Indicator	Definition/Unit	Expected effect
Absorption	A1	Source-sink landscape mean distance	Mean distance between grey "source" patches and nearest blue-green "sink" patches (m)	–
	A2	Impervious surface ratio	Impervious surface as % of total area	–
	A3	Normalized Difference Vegetation Index (NDVI)	Mean NDVI (unitless)	+
	A4	Relief variation	Mean local elevation range (m)	+
	A5	Open water ratio	Rivers + lakes + reservoirs as % of total area	+
	A6	Wetland ratio	Wetlands as % of total area	+
Coping	B1	Open space area	Total public/open space (km^2)	+
	B2	Emergency shelter capacity	Available shelter places (persons)	+
	B3	Typhoon-rainstorm-urban waterlogging sensitivity	Sensitivity to Typhoon-Rainstorm-Urban waterlogging chain (dimensionless)	-
	B4	Flood control facility coverage	Flood protection works as % of total area	+
	B5	Vulnerable population share	Population ≤ 14 yr + ≥ 65 yr as % of total	–
	B6	Storm surge protection coverage	Surge barrier works as % of total area	+
	B7	Typhoon-rainstorm-flooding sensitivity	Sensitivity to Typhoon-Rainstorm-Flooding chain (dimensionless)	–
	B8	Typhoon-strong wind-storm surge sensitivity	Sensitivity to Typhoon-Strong wind-Storm surge chain (dimensionless)	–
Recovery and adaptation	C1	Land use diversity	Count of land use categories	+
	C2	Intersection density	Road intersections per km^2	+
	C3	Accessibility index	Mean travel time accessibility (unitless)	+
	C4	Road density	Road length per km^2	+
	C5	Economic density	GDP per km^2 (10^3 CNY per km^{-2})	+
	C6	Population density	Residents per km^2	–
	C7	Medical resource coverage	Hospital beds per 10,000 residents	+

"Expected effect" indicates the direction of influence on resilience: "+" enhances, "–" diminishes

weight-perturbation analysis constitute the response vector y.

Step 2: Model training and validation. An XGBoost regression model is trained using the objective function:

$$L(\theta) = \sum_i (y_i - \hat{y}_i)^2 + \Omega(\theta), \tag{6}$$

where $\Omega(\theta)$ represents regularization terms. Model performance is evaluated using root mean squared error (RMSE) and R^2 on a hold-out test dataset, ensuring adequate predictive accuracy for subsequent diagnostic analysis.

Step 3: Global association analysis. SHAP values are computed using the TreeSHAP algorithm to decompose model predictions into additive contributions from individual indicators:

$$\hat{y} = \phi_0 + \sum_{j=1}^{21} \phi_{ij}, \tag{7}$$

where ϕ_{ij} represents the SHAP value of indicator j for grid cell i. Indicator-TDCUR association strength is summarized using mean absolute SHAP values, reflecting the relative contribution of each indicator to model predictions under the established TDCUR framework.

Step 4: Interaction and threshold diagnosis. Pairwise SHAP interaction values are examined to identify dominant interaction structures among indicators. In addition, segmented regression is applied to SHAP dependence relationships to detect changes in association slopes across indicator value ranges. These thresholds are interpreted as empirical turning points in the model response surface, rather than physical or causal thresholds inherent to the TDCUR formulation.

Step 5: Multi-scale spatial diagnosis. Absolute SHAP values ($\sum |SHAP|$) are aggregated from grid to county, city, and basin scales to identify spatial areas where multiple indicators jointly exhibit strong associations with low TDCUR values. This aggregation provides diagnostic information to support spatial prioritization within the existing TDCUR assessment framework, without redefining resilience levels or intervention priorities.

Importantly, SHAP-based metrics in this study are interpreted as descriptors of spatial association patterns and nonlinear responses under the predefined TDCUR formulation.

They do not alter indicator weights, modify index construction, or imply causal relationships.

3 Results

This section first reports the spatiotemporal patterns of typhoon disaster chain urban resilience (TDCUR) across Fujian Province and examines changes from 2010 to 2020. It then identifies resilience hot spots and cold spots and their temporal evolution. Finally, XGBoost-SHAP is used as a diagnostic tool to characterize nonlinear indicator-TDCUR associations and interactions under the predefined TDCUR formulation and to identify areas where multiple indicators jointly align with low TDCUR.

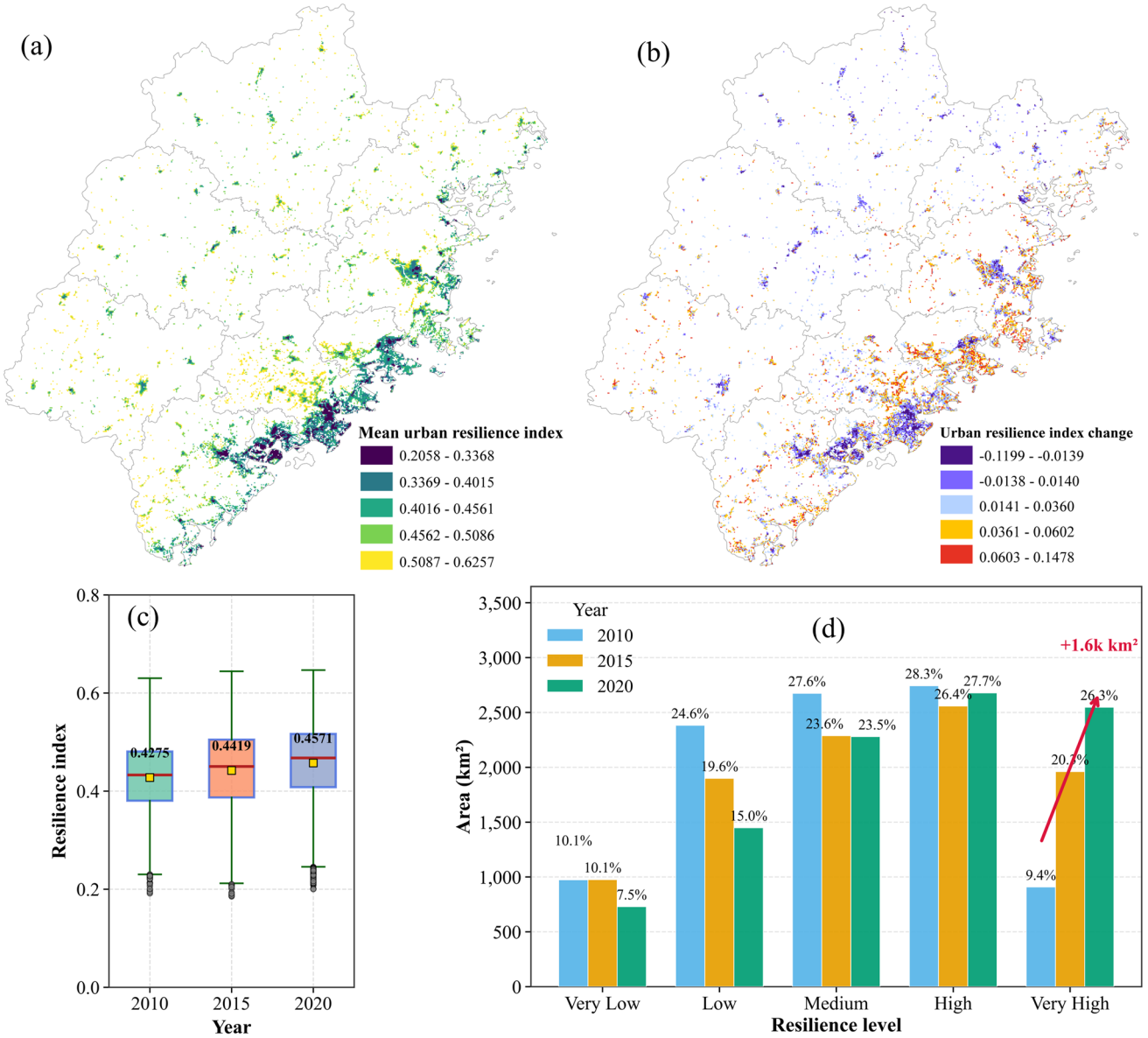


Fig. 3 Spatial and temporal patterns of typhoon disaster chain urban resilience (TDCUR) across Fujian Province, China, 2010–2020. **a** Mean urban resilience index, averaged for 2010–2020; **b** Change in urban resilience index between 2010 and 2020; **c** Interannual variability of the urban resilience index (2010, 2015, and 2020) illustrated by boxplots; **d** Areal extent (km^2) of different urban resilience classes (Very Low, Low, Medium, High, Very High) from 2010 to 2020. Resilience classes were defined following the risk grading criteria of China's First National Comprehensive Risk Survey of Natural Disasters. All interannual comparisons (2010, 2015, 2020) were conducted within the fixed 2020 delineated urban extent to ensure spatial comparability

3.1 Spatiotemporal Patterns of Urban Resilience to Typhoon Disaster Chains

The analysis revealed a clear east-west gradient in TDCUR across Fujian Province, with higher TDCUR values (indicating stronger resilience) in western areas and lower values in the eastern coastal belt (Fig. 3a). Notably, lower resilience values were observed primarily in the core urban zones of Fuzhou, Quanzhou, and Xiamen, rather than in less developed areas. These urban cores also tended to coincide with very high impervious-surface coverage (> 85%) and older built-environment conditions, which is consistent with lower absorption and coping capacity reflected in the predefined TDCUR framework. Between 2010 and 2020, the provincial average TDCUR increased from 0.4275 to 0.4571, representing a 6.9% improvement (Fig. 3c), while areas classified as very high resilience expanded by 1,638.6 km^2 within the fixed 2020 urban extent (Fig. 3d). During the same period, core districts in major coastal cities exhibited a declining trend in resilience (for example, Gulou and Taijiang in Fuzhou, and Siming and Huli in Xiamen), suggesting a potential divergence between conventional urban development and resilience enhancement (Fig. 3b). Kernel density estimation further demonstrated that the peak of the TDCUR distribution shifted from 0.47 in 2010 to 0.51 in 2015, stabilizing at 0.50 in 2020—a net increase of approximately 6.4% over the decade. Concurrently, the distribution width narrowed by approximately 22% (Fig. 4j), indicating both an overall improvement in TDCUR and a reduction in regional disparities.

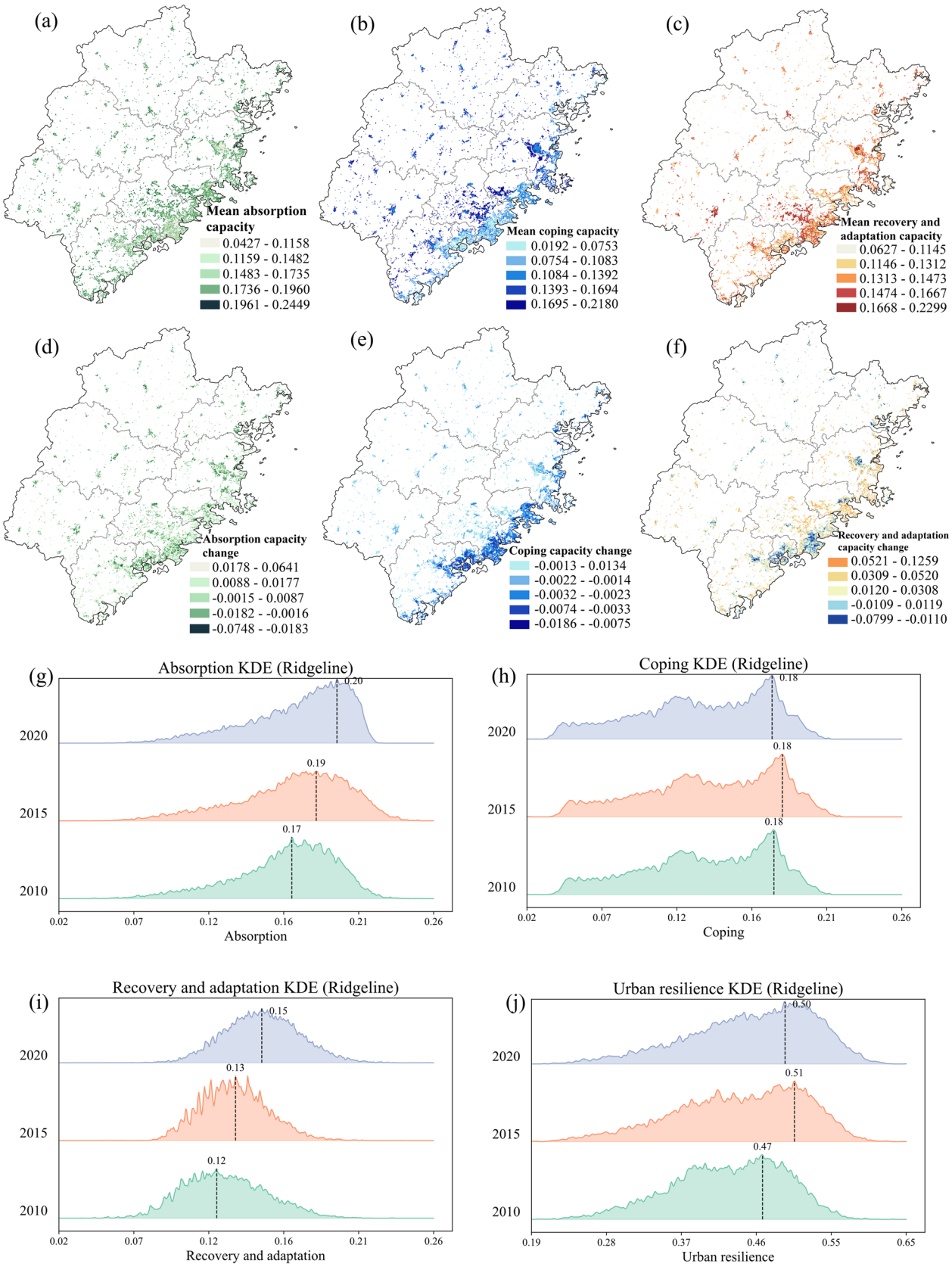
Based on the three constituent capacities of TDCUR (Fig. 4), western cities generally exhibited higher absorption and coping capacities, which is consistent with their overall higher resilience levels. In contrast, the eastern coastal core areas showed comparatively lower absorption and coping capacities. Specifically, the median absorption capacity in Jinjiang was 0.103, 58% lower than the provincial maximum (0.245), and its minimum grid-level value was only 17.4% of the maximum (Fig. 4a). Coping capacity in Siming and Huli Districts (Xiamen) and Jinjiang declined from 2010 to 2020 (Fig. 4e) and was approximately 40–50% lower in 2020 than in comparable inland areas (Fig. 4b). Although coastal core zones maintained the highest recovery and adaptation capacity, most gains from 2010 to 2020 occurred in inland cities, while coastal urban centers showed limited improvement (Fig. 4c, f). Kernel density estimation further indicated that the absorption capacity peak increased from 0.16 to 0.20, accompanied by an extended lower tail (Fig. 4g). The mean coping capacity remained around 0.18, but its distribution widened and shifted downward in coastal cores (Fig. 4h). Meanwhile, the recovery and adaptation peak rose from 0.12 to 0.15 with a more balanced spatial distribution, suggesting a diffusion of improvements from coastal to inland areas (Fig. 4i). Taken together, these results suggest that narrowing the coping capacity gap in coastal core areas may warrant priority attention for improving overall resilience.

There is often a scale mismatch between detailed assessment results and comprehensive governance decisions, making direct translation of findings difficult. To address this, we aggregated the 30-arc-second TDCUR data to county, city, and basin units, systematically revealing the spatiotemporal heterogeneity of resilience across scales. A consistent "low in the east, high in the west" pattern was observed at all scales, indicating widespread resilience deficits in the economically dense eastern coastal zone. At the county level, the five weakest counties were all located in the east, with an average value only 57.8% of that of the top western counties (for example, Yongding District, 0.5016). The improvement in some coastal non-core counties (for example, Jimei District, +0.0079) suggests a positive regional synergy effect (Fig. 5a, d). At the city level, Xiamen exhibited the lowest resilience (0.3252), while Putian achieved the fastest growth (+0.0166), reflecting divergent resilience trajectories across urban development paths (Fig. 5b, e). On the basin scale, the coastal directly discharging composite (CS) basin showed the lowest resilience (0.3710). In contrast, the Jinjiang Basin demonstrated the most rapid increase (+0.0269), highlighting the potential benefits of integrated basin management (Fig. 5c, f). The multi-scale analysis not only validated previous findings but also delineated a typical divergence pattern: improvement in non-core coastal areas, stability in high-resilience inland zones, and decline in core urban districts, providing a critical basis for differentiated spatial governance strategies.

3.2 Spatial Patterns and Dynamics of Urban Resilience Hot Spots

Based on Getis-Ord Gi* analysis, TDCUR in Fujian Province exhibited a distinct "clustered low resilience, dispersed high resilience" spatial pattern (Fig. 6a). Statistically significant cold spots dominated this distribution, covering 447 km^2 (4.6% of the study area), with over 80% concentrated in the Xiamen-Quanzhou urban core. In contrast, hot spots were limited to 18 km^2 (0.2%) and sporadically distributed across inland cities. Between 2010 and 2020, the cold spot area expanded by 48%, while hot spot area contracted by 51%, indicating intensifying clustering of low-resilience areas alongside contraction of high-resilience zones (Fig. 7a).

Local Moran's I analysis confirmed a persistent coastal belt of low-low (LL) resilience clustering (Fig. 6b). From 2010 to 2020, the LL cluster area decreased by 243.7 km^2 (−10.0%), while high-high (HH) clusters showed a modest reduction of 6.4%. Both low-high (LH) and high-low (HL) spatial outliers remained below 3% throughout the study


(a)
Mean absorption capacity
0.0427 - 0.1158
0.1159 - 0.1482
0.1483 - 0.1735
0.1736 - 0.1960
0.1961 - 0.2449
(b)
Mean coping capacity
0.0192 - 0.0753
0.0754 - 0.1083
0.1084 - 0.1392
0.1393 - 0.1694
0.1695 - 0.2180
(c)
Mean recovery and adaptation capacity
0.0627 - 0.1145
0.1146 - 0.1312
0.1313 - 0.1473
0.1474 - 0.1667
0.1668 - 0.2299
(d)
Absorption capacity change
0.0178 - 0.0641
0.0088 - 0.0177
-0.0015 - 0.0087
-0.0182 - -0.0016
-0.0748 - -0.0183
(e)
Coping capacity change
-0.0013 - 0.0134
-0.0022 - -0.0014
-0.0032 - -0.0023
-0.0074 - -0.0033
-0.0186 - -0.0075
(f)
Recovery and adaptation capacity change
0.0521 - 0.1259
0.0309 - 0.0520
0.0120 - 0.0308
-0.0109 - 0.0119
-0.0799 - -0.0110
(g)
Absorption KDE (Ridgeline)
2020
2015
2010
0.20
0.19
0.17
0.02 0.07 0.12 0.16 0.21 0.26
Absorption
(h)
Coping KDE (Ridgeline)
2020
2015
2010
0.18
0.18
0.18
0.02 0.07 0.12 0.16 0.21 0.26
Coping
(i)
Recovery and adaptation KDE (Ridgeline)
2020
2015
2010
0.15
0.13
0.12
0.02 0.07 0.12 0.16 0.21 0.26
Recovery and adaptation
(j)
Urban resilience KDE (Ridgeline)
2020
2015
2010
0.50
0.51
0.47
0.19 0.28 0.37 0.46 0.55 0.65
Urban resilience

◂**Fig. 4** Spatial patterns and ridgeline kernel density estimation (KDE) of the three resilience capacities in Fujian Province, 2010–2020. **a**, **d**, **g** Absorption: mean, change, KDE; **b**, **e**, **h** Coping: mean, change, KDE; **c**, **f**, **i** Recovery and adaptation: mean, change, KDE; **j** Overall resilience: Typhoon disaster chain urban resilience (TDCUR) KDE

period. These patterns suggest that while coastal resilience deficits remained substantial, they were showing signs of spatial convergence, with high-resilience cores maintaining stability and low-resilience clustering gradually weakening (Fig. 7c, d).

Spatiotemporal classification revealed three distinct cold spot trajectories (Figs. 6c and 7b): persistent cold spots (43.8% of classified areas) remained concentrated along the Xiamen-Zhangzhou-Quanzhou coastline; diminishing cold spots (4.0%), primarily in inland counties, demonstrated clear resilience recovery; and emerging cold spots (2.4%), distributed along urban fringes, signaled potential future vulnerability. Collectively, these findings systematically characterize the spatial organization and evolutionary pathways of urban resilience, providing a robust foundation for developing targeted intervention strategies.

3.3 Diagnostic Analysis of Indicator-Typhoon Disaster Chain Urban Resilience (TDCUR) Associations Using XGBoost and SHapley Additive exPlanations (SHAP)

To examine indicator-TDCUR association patterns under the predefined TDCUR formulation, we fitted an XGBoost model using grid-level data from 2010, 2015, and 2020, with a 70:30 split for training and testing. Hyperparameters were tuned by grid search with five-fold cross-validation (subsample = 0.6, colsample_bytree = 0.8, max_depth = 6, n_estimators = 600, learning_rate = 0.05, min_child_weight = 1, reg_alpha = 0.5, reg_lambda = 1.0, gamma = 0). The model showed strong performance on the test set ($R^2 = 0.9932$; RMSE = 0.0062; mean absolute error (MAE) = 0.0043), enabling SHAP-based diagnostics.

SHapley Additive exPlanations was used to summarize how indicator values relate to predicted TDCUR within the fitted model (Fig. 8). Typhoon-strong wind-storm surge sensitivity (B8) had the highest mean absolute SHAP value in the fitted model (23.52%), followed by typhoon-rainstorm-flooding sensitivity (B7, 15.72%) and impervious surface ratio (A2, 10.06%) (Fig. 8a). High values of these indicators were mainly concentrated in the urban cores of Xiamen and Quanzhou, which also showed lower TDCUR and weaker absorption and coping capacities. SHAP summary and dependence plots indicate generally negative associations for B8, B7, and A2, while C4 showed a positive association pattern (Fig. 8b–f). Piecewise linear fits identified significant slope changes ($\Delta\beta$, $p < 0.05$) at B8 = −0.60, B7 = −0.66, A2 = −0.79, and C4 = 0.14 (Fig. 8c–f), indicating nonlinearity in the fitted associations across value ranges. These values reflect features of the fitted response and are not physical or regulatory thresholds. These magnitudes reflect model-based explanations and do not alter the predefined TDCUR calculation.

We further examined pairwise SHAP interactions across all 21 indicators (231 pairs). For each pair, we calculated the mean absolute interaction value (|ϕ|) with a 95% bootstrap confidence interval (2,000 resamples) and ranked pairs accordingly. The strongest interaction was B7 × B8 ($|\phi| = 1.88 \times 10^{-3}$; 22.0% of the total among the top 10 pairs), followed by A2 × B7 (1.18×10^{-3}, 13.8%), A2 × B8 (1.03×10^{-3}, 12.0%), A4 × B8 (7.71×10^{-4}, 9.0%), and A3 × B7 (7.39×10^{-4}, 8.6%). Figure 9 shows six representative pairs. Five pairs are significant (Fig. 9a–c, e–f), while A4 × B8 is not significant based on the bootstrap test (Fig. 9d). For most high-ranking pairs (for example, B7 × B8 and A2 × B7), interaction values are mostly negative, meaning that high values of both indicators tend to coincide with lower predicted TDCUR in the fitted model.

Finally, we summed absolute SHAP values (Σ|SHAP|) within each grid cell and aggregated them at county, city, and basin scales to summarize areas where multiple indicators jointly show stronger model-based associations with low TDCUR (Fig. 10). High Σ|SHAP| values are consistently concentrated along the Xiamen-Quanzhou-Fuzhou coastal belt. At the county level, Huli, Taijiang, and Gulou have mean Σ|SHAP| values above 0.18. At the city level, Xiamen, Quanzhou, and Fuzhou rank highest. At the basin scale, the Jinjiang, Minjiang, CS, and Jiulongjiang basins average about 0.145 (Fig. 10a, c, e). As a robustness check, we repeated the analysis using five indicators (B8, B7, A2, A4, A3). Mean Σ|SHAP| decreased by only 3–5% across scales, and spatial rankings remained highly consistent (Spearman $\rho \approx 0.96$) (Fig. 10b, d, f). This consistency suggests that the reduced indicator set preserves the main spatial contrasts in Σ|SHAP|, supporting the robustness of the SHAP-based spatial diagnostics under the predefined TDCUR framework.

4 Discussion

This section interprets the spatiotemporal and multi-scale TDCUR patterns, discusses their implications for resilience planning, and outlines the methodological limitations and priorities for further research.

4.1 Applicability of the Framework

The application of the 30-arc-second grid-based typhoon disaster chain urban resilience (TDCUR) assessment framework in Fujian Province reveals that the economically

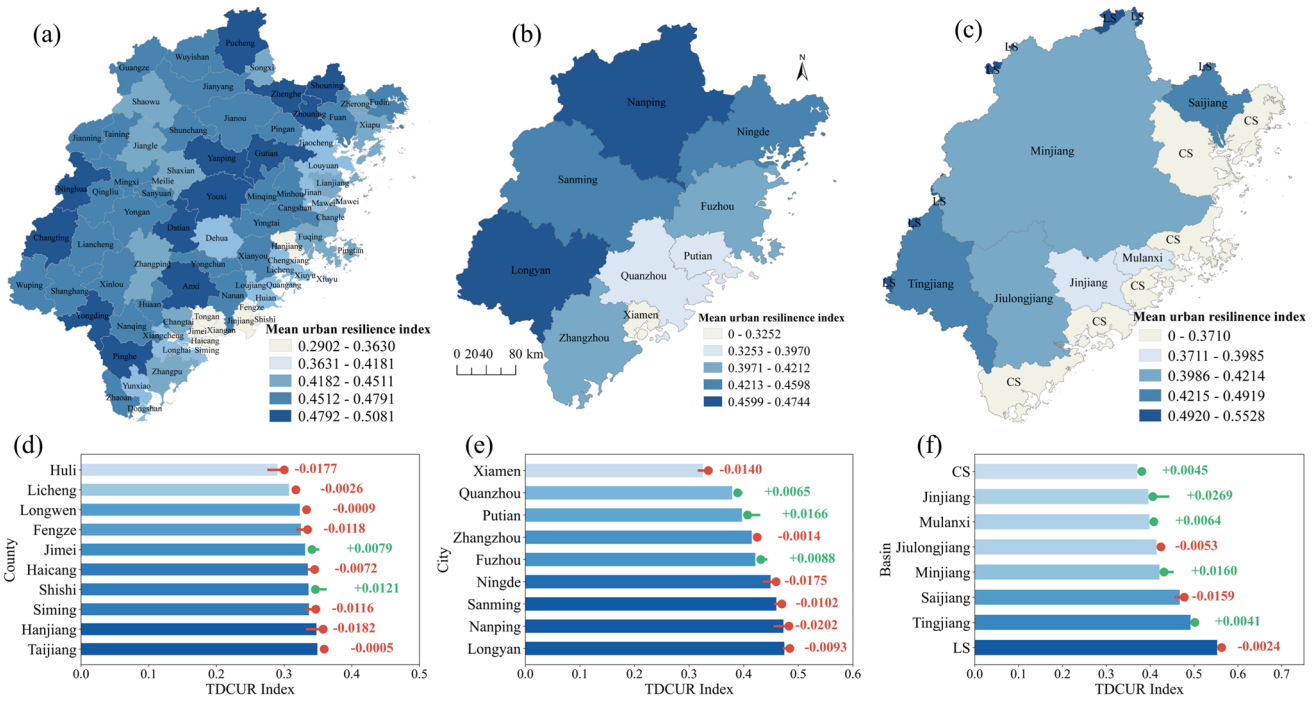


Fig. 5 Multi-scale spatial distribution and ranking of typhoon disaster chain urban resilience (TDCUR) in Fujian Province (county, city, and basin levels). **a** County-level mean resilience index; **b** City-level mean resilience index; **c** Basin-level mean resilience index. Panels **d**–**f** combine bar charts of 2020 mean TDCUR with overlaid dots showing the absolute change in TDCUR from 2010 to 2020: green dots (and labels) denote gains, red dots denote declines. Specifically, panel **d** ranks the top 10 counties and their change in TDCUR; panel **e** displays all cities and their change in TDCUR; and panel **f** displays all basins and their change in TDCUR—highlighting spatial resilience patterns and which jurisdictions had improved or deteriorated over the decade

developed urban cores of Fuzhou, Quanzhou, and Xiamen did not exhibit higher resilience levels; instead, they showed characteristics of systemic resilience deficits. This finding contrasts with the common expectation that economic development inherently ensures greater resilience (Bristow and Healy 2018; Zhu et al. 2021). This discrepancy may stem from three interrelated factors. First, infrastructure systems in older urban areas—such as drainage and disaster prevention facilities—were designed to outdated standards and struggle to cope with the compound pressures of high population density, asset concentration, and increasingly intense typhoon disaster chains. These areas are characterized by high sensitivity to typhoon-rainstorm-urban waterlogging (B3) and typhoon-strong wind-storm surge (B8), both of which are strongly associated with low TDCUR values. Second, infrastructure renewal and upgrading efforts have lagged behind evolving risk conditions. Third, the coastal location entails high exposure to typhoons and associated compound hazards, which, combined with dense populations and economic activities, further constrains overall coping capacity (Yang et al. 2025).

Spatially, TDCUR in Fujian exhibited a distinct "high in the west, low in the east" pattern, alongside a provincial trend of overall improvement and narrowing regional disparities. The western region's higher resilience likely relates to its lower urbanization intensity, superior natural ecological conditions (reflected by higher Normalized Difference Vegetation Index, A3), and more dispersed population and assets, which collectively enhance absorption and coping capacities. In contrast, intense development in the eastern region increases exposure (for example, high A2) and sensitivity (for example, high B3, B7, B8), leading to comparatively weaker absorption and coping capabilities.

Compared to studies relying on single administrative units, the multi-scale assessment framework developed here offers distinct advantages (Xie et al. 2023; Liu et al. 2024). It effectively identifies fine-grained resilience variations masked by unit-level averages, precisely locating persistent low-resilience areas. This provides a spatial basis for prioritizing infrastructure upgrades or ecological restoration in key grid cells. Simultaneously, by aggregating data to county, city, and basin scales, the framework helps disaster management authorities at different levels identify critical weaknesses within their jurisdictions, supporting optimized resource allocation and cross-level coordination.

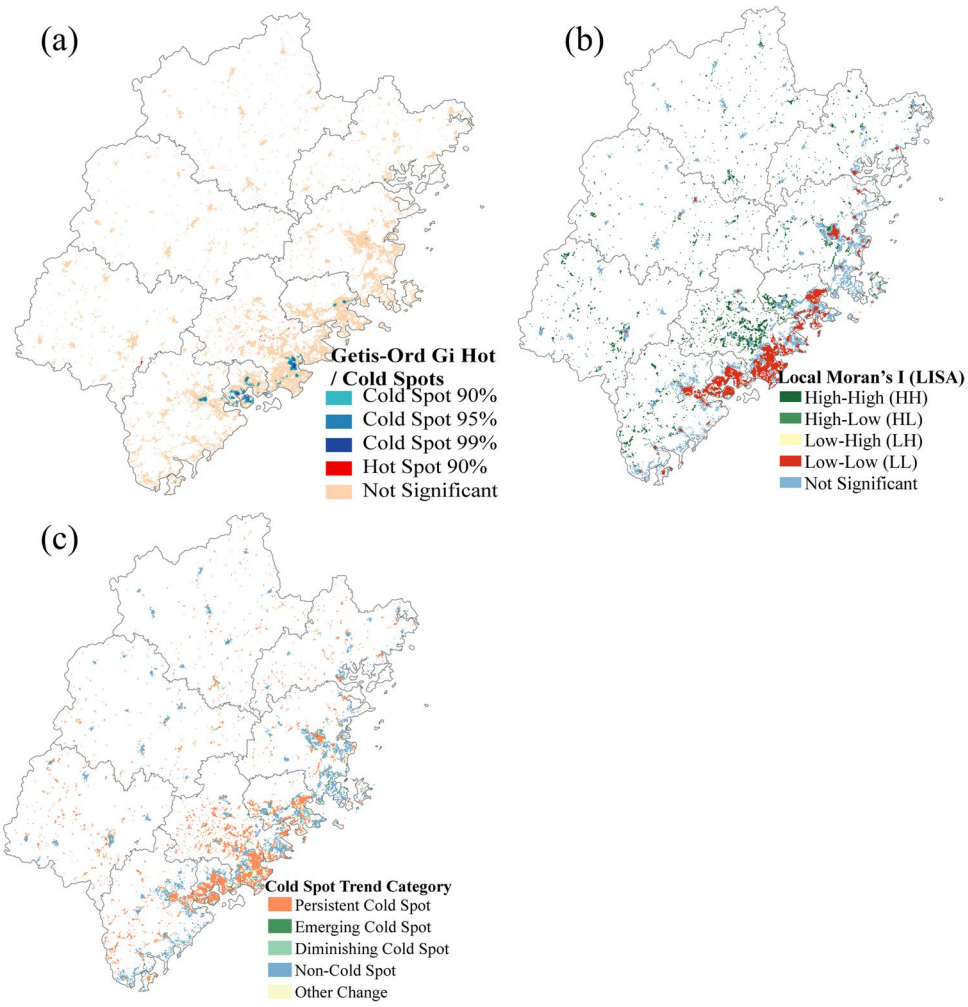


Fig. 6 Spatial clusters of typhoon disaster chain urban resilience (TDCUR) in Fujian Province, 2010–2020. **a** Getis-Ord Gi hot spots and cold spots in 2020; **b** Local Moran's I cluster types (HH, LL, HL, LH) in 2020; **c** Spatiotemporal cold spot trend categories across 2010, 2015, and 2020

4.2 Improvement Strategies

Based on the multi-scale TDCUR results, this study outlines targeted pathways for resilience enhancement. Across scales, the Xiamen-Quanzhou-Fuzhou coastal belt consistently emerges as a concentrated low-resilience area. Persistent cold spots—representing 43.8% of the classified area and including Siming and Huli Districts in Xiamen, Jinjiang City in Quanzhou, and Gulou and Taijiang Districts in Fuzhou—should be considered focal areas for action (Lin, He, et al. 2022; Lin, Peng, et al. 2022; Massaro et al. 2023; Shafiei-Dastjerdi and Lak 2023). Given their high impervious surface ratios (A2 > 85%), nature-based and low-impact measures such as rain gardens and permeable pavements can be implemented to enhance infiltration and reduce pluvial flooding pressure.

SHapley Additive exPlanations interaction results further show that B7, B8, and A2 tend to co-occur in low-TDCUR areas. This pattern supports considering integrated measures in coastal cores—combining drainage system upgrading, storm surge defense enhancement, and impervious surface management—to address compound pressures associated with typhoon-rainstorm-flood and typhoon-strong wind-storm surge chains under the existing assessment framework (Chatti and Majeed 2022; Agboola and Tunay 2023; Sun et al. 2023).

For inland areas with higher resilience, maintaining ecological conditions remains important. Higher NDVI values (A3; mean absorption capacity ≈ 0.245) underscore the role of ecological conservation measures in sustaining natural buffering functions. Locating regional emergency supply centers in areas such as Yongding District (Longyan) could leverage geographic advantages to support post-disaster response for coastal zones (AghaKouchak et al. 2018; Tiggeloven et al. 2020; Mallick et al. 2021). In addition, turning points in the fitted associations (for example, A2 = −0.79, roughly corresponding to ~85% imperviousness) provide a useful reference point for discussing development intensity in urban planning.

A dynamic monitoring system based on multi-source data is recommended, focusing on three representative area types: persistent cold spots (for example, the coastal corridor from

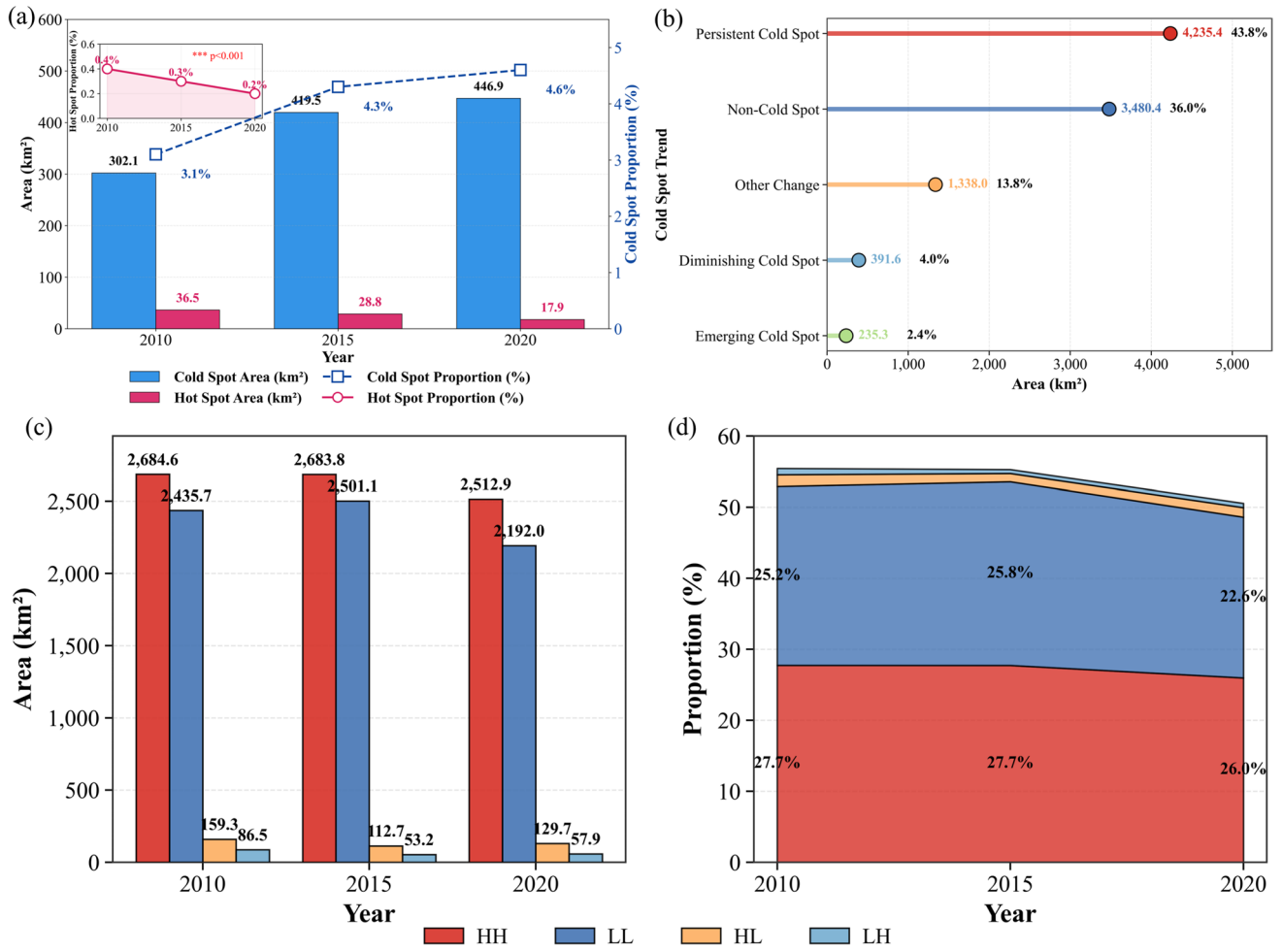


Fig. 7 Temporal dynamics of spatial clustering patterns of typhoon disaster chain urban resilience (TDCUR) in Fujian Province, 2010–2020. **a** Changes in area of Getis-Ord Gi hot spots and cold spots, 2010–2020; **b** Areas and percentages of cold spot trend categories, 2010–2020; **c** Changes in area of local Moran's I cluster types, 2010–2020; **d** Proportions of local Moran's I cluster types, 2010–2020

Xiamen to Zhangzhou and Quanzhou), emerging cold spots (for example, urban fringes), and diminishing cold spots (for example, certain inland counties). Core metrics should track temporal changes in coping and absorption capacities. Periodic SHAP analysis can be used to track changes in model-based association patterns over time and around major interventions, providing supporting evidence for iterative refinement of resilience strategies (Mallick et al. 2021; Chatti and Majeed 2022; Pee and Pan 2022).

4.3 Limitations and Future Research

This study has several limitations. First, although proxy indicators such as impervious surface ratio (A2) and flood control facility coverage (B4) ensure multi-scale comparability and data accessibility—particularly for characterizing coping capacity related to urban waterlogging risk—they do not support engineering grade precision. Nevertheless, the approach effectively reveals systematic spatial patterns of resilience deficits across governance scales, fulfilling its role as a macroscopic screening and comparison tool. Future studies could focus on critical cold spots (for example, Siming District and Gulou District) by incorporating detailed drainage network data to advance from macro-scale pattern recognition to micro-scale mechanistic analysis. Second, the current framework covers three typhoon disaster chains involving rainfall, flooding, urban waterlogging, strong winds, and storm surges; future research should incorporate additional cascading hazards, such as landslides, to broaden the multi-hazard assessment. Third, the three capacity partition (absorption, coping, and recovery and adaptation) is used as an operational structure for organizing indicators and reporting results; future work can further examine its robustness against alternative resilience typologies. Finally, because grid-level observations exhibit spatial dependence, the random train-test split and conventional cross-validation

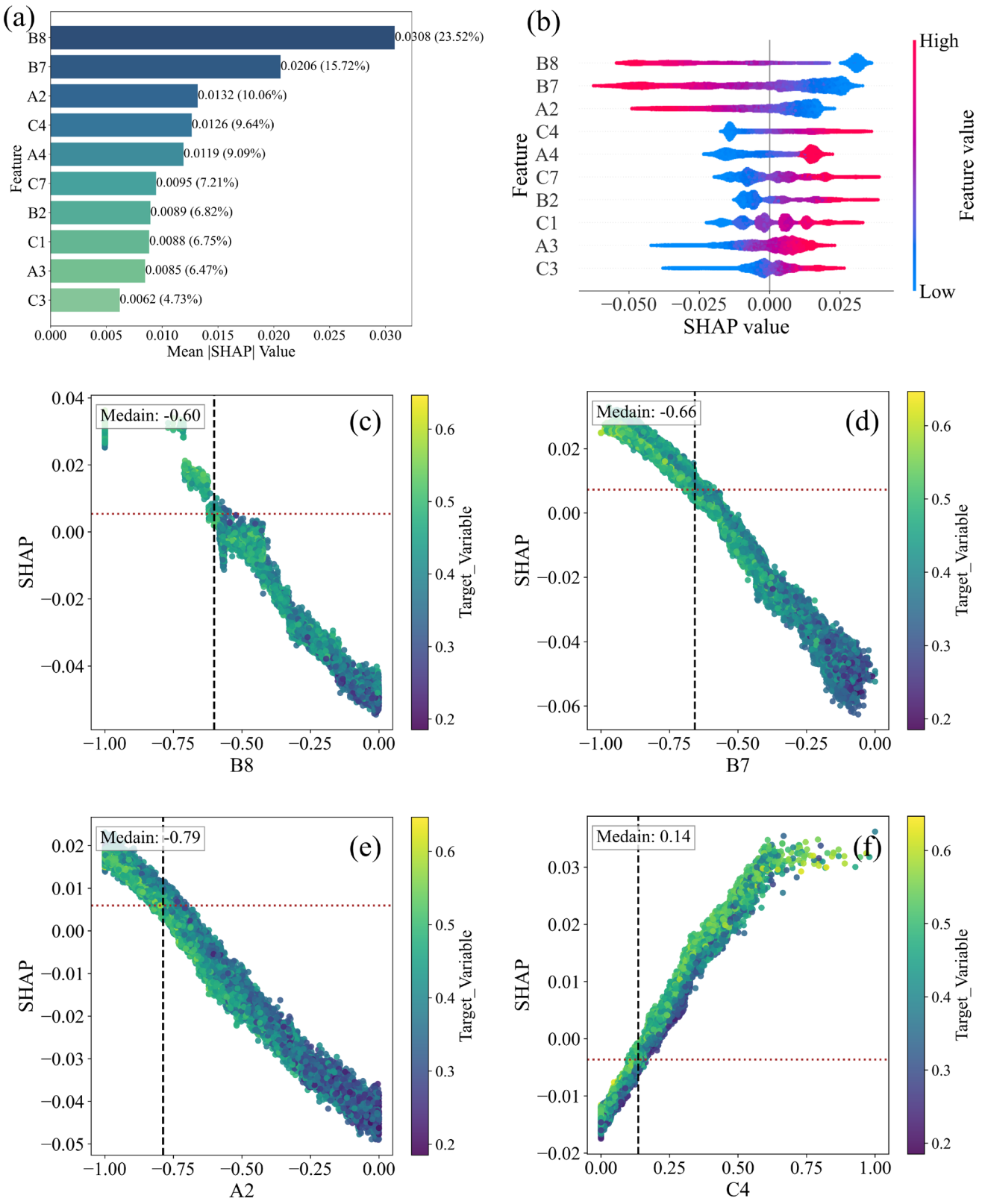


Fig. 8 SHapley Additive exPlanations (SHAP)-based diagnostics for the XGBoost-typhoon disaster chain urban resilience (TDCUR) model in Fujian Province. **a** Mean absolute SHAP values for the 10 features with the highest values in the fitted model; **b** SHAP summary plot for these features; **c–f** SHAP dependence plots for B8, B7, A2, and C4

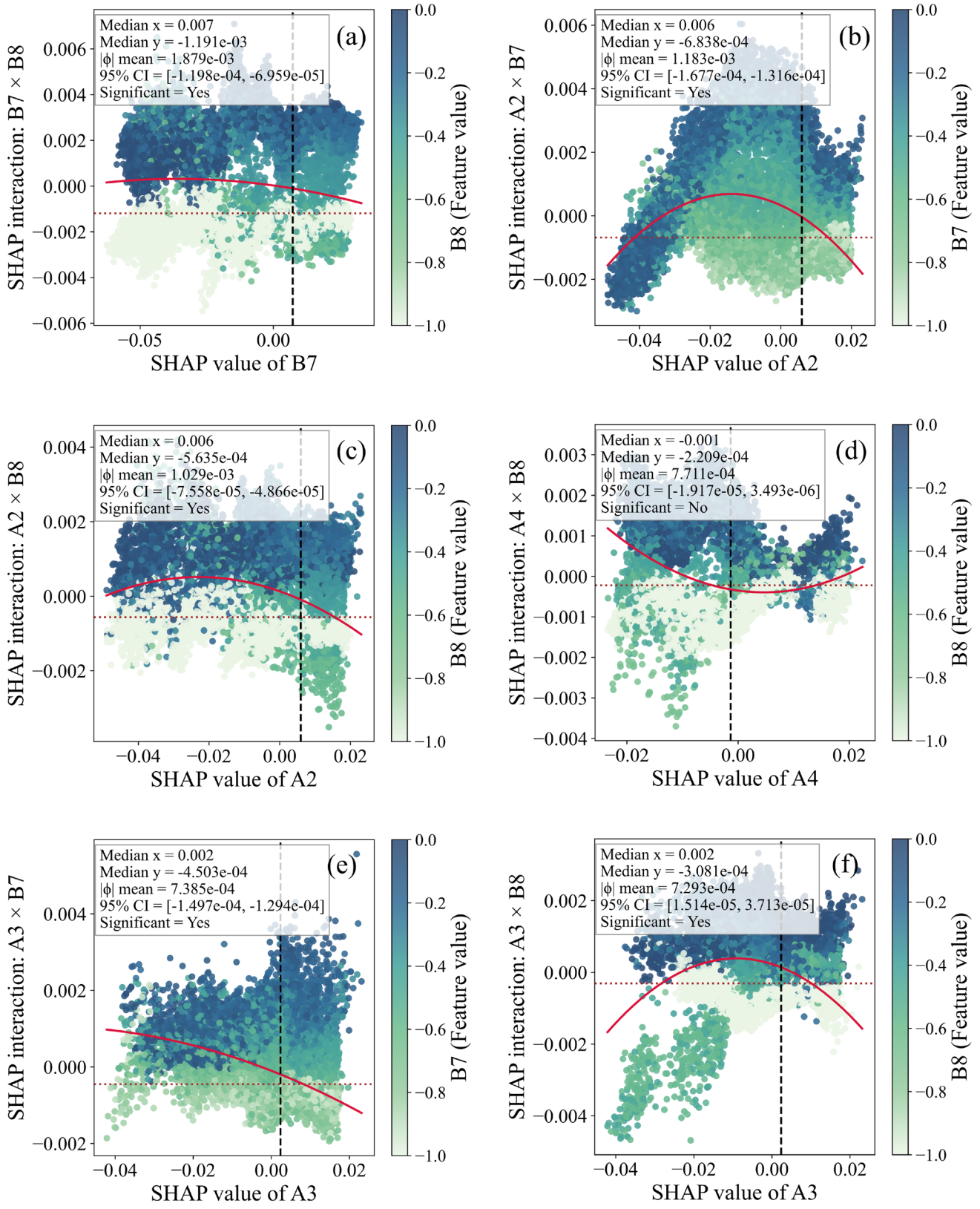


Fig. 9 SHapley Additive exPlanations (SHAP) interaction diagnostics for typhoon disaster chain urban resilience (TDCUR): Six highest-ranked indicator pairs by mean absolute SHAP interaction value (|ϕ|)

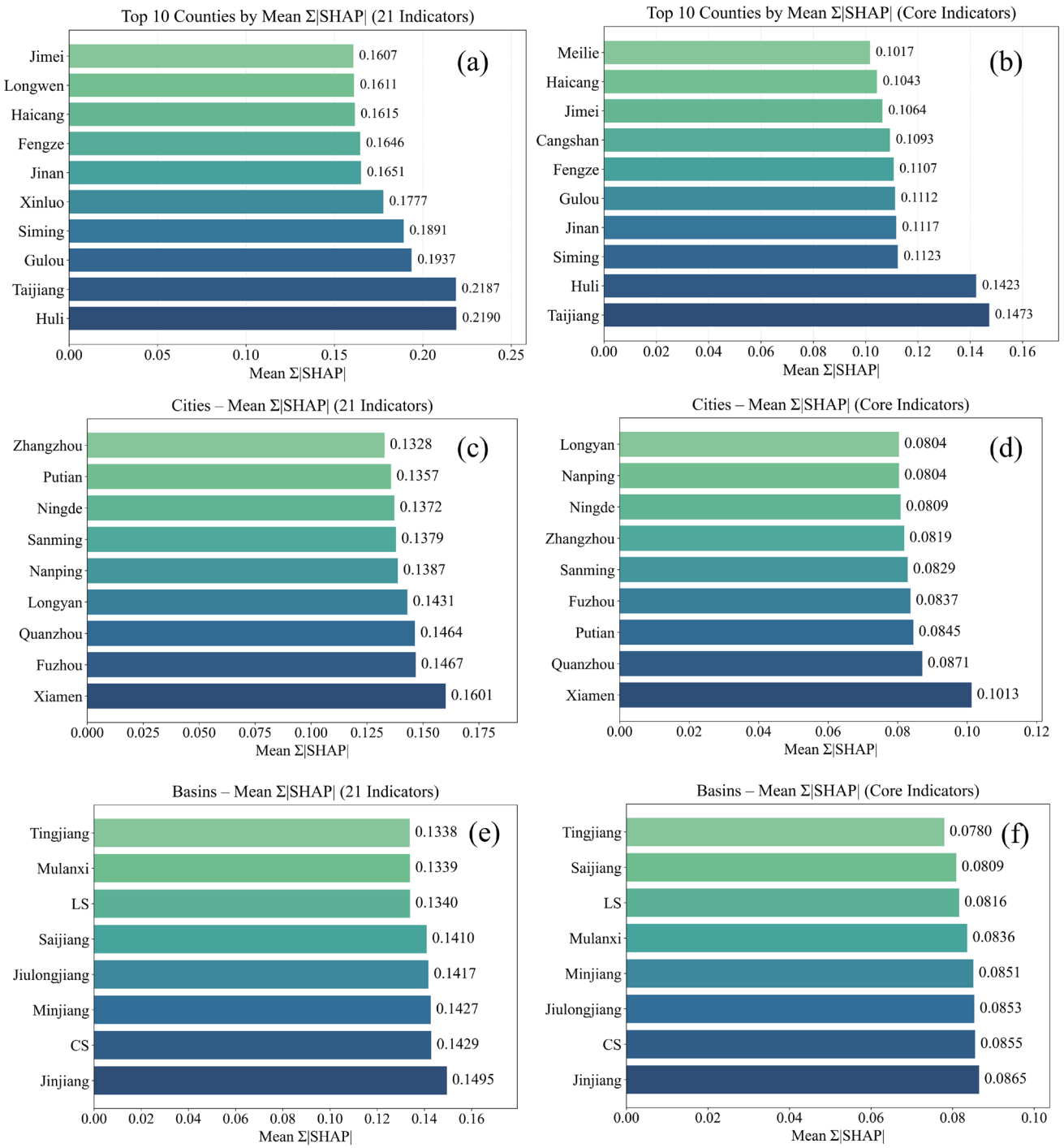


Fig. 10 Multi-scale summaries of cumulative SHapley Additive exPlanations (SHAP) magnitudes (mean Σ|SHAP|) under the fitted model. **a**, **c**, **e** Results using all 21 indicators; **b**, **d**, **f** results using the core indicator set. Panels show counties, cities, and basins, respectively

used for XGBoost may yield optimistic fit statistics. Future work can adopt spatial blocking or spatial cross-validation to more strictly assess out-of-area model performance. Overall, the proposed multi-scale framework and the resilience heterogeneity patterns identified in this study provide a scientific basis for targeted governance and further investigation.

5 Conclusion

This study developed a multi-scale assessment framework to quantify typhoon disaster chain urban resilience (TDCUR) in Fujian Province from 2010 to 2020 at grid, administrative unit, and watershed scales. XGBoost-SHAP was further

used as a diagnostic tool to identify model-based indicator-TDCUR association patterns. The main conclusions are as follows:

(1) From 2010 to 2020, provincial TDCUR increased slowly, with the mean value rising from 0.4275 to 0.4571. This indicates an overall improvement in resilience and a modest reduction in regional disparities. However, resilience decreased in several economically developed coastal cities (Fuzhou, Quanzhou, and Xiamen), showing that economic growth and resilience improvement did not change in a simple synchronous way during the study period.

(2) Across scales, TDCUR showed a stable spatial gradient of "high in the west and low in the east." At the county scale, the mean resilience in Huli District (Xiamen) was 57.8% of that in Yongding District (Longyan; 0.5016). At the city scale, Xiamen had the lowest resilience (0.3252). At the watershed scale, resilience in the Jinjiang River Basin increased by 0.0269, which is about 1.6 times the provincial mean increase.

(3) Spatial clustering results indicate that low-resilience areas remained concentrated along the coast. The cold spot area expanded by 48% to 447 km^2, and about 80% of this area was located along the Xiamen-Quanzhou coastal belt. In contrast, the area of high-resilience hot spots decreased by 51% to 18 km^2, suggesting increasing spatial polarization in coastal resilience.

(4) The machine learning diagnosis indicates that typhoon-strong wind-storm surge sensitivity (B8), typhoon-rainfall-flooding sensitivity (B7), and impervious surface ratio (A2) had the strongest model-based associations with the spatial variation of TDCUR. Their mean absolute SHAP contributions were 23.52%, 15.72%, and 10.06%, respectively. The fitted association patterns showed clear turning points near $B8 = -0.60$, $B7 = -0.66$, and $A2 = -0.79$. In SHAP interaction analysis, $B7 \times B8$ ranked first (22% of the top 10 interaction strength), indicating a strong joint association pattern between the two sensitivities in the fitted model.

(5) The spatial aggregation of $\Sigma|SHAP|$ shows that the Xiamen-Quanzhou-Fuzhou coastal belt and the Jinjiang River Basin consistently had the highest cumulative model-based association magnitudes across scales. These regions should be prioritized in resilience planning and resource allocation.

Overall, the integrated multi-scale assessment-machine learning diagnosis-spatial identification framework provides methodological support for systematic evaluation of typhoon disaster chain resilience in coastal regions. The findings also support differentiated, region-specific strategies for resilience improvement.

Acknowledgments This work was supported by the National Natural Science Foundation of China (Grant No. 42271030), the "Young Eagle Plan" Top Talents Program of Fujian Province, and the KARE II project funded by the German Federal Ministry of Education and Research (BMBF; Grant No. 01LR2006D1). Jianhui Wei received support through the KARE II project. Lu Gao was supported by an Alexander von Humboldt Foundation Research Fellowship for Experienced Researchers.

Open Access This article is licensed under a Creative Commons Attribution 4.0 International License, which permits use, sharing, adaptation, distribution and reproduction in any medium or format, as long as you give appropriate credit to the original author(s) and the source, provide a link to the Creative Commons licence, and indicate if changes were made. The images or other third party material in this article are included in the article's Creative Commons licence, unless indicated otherwise in a credit line to the material. If material is not included in the article's Creative Commons licence and your intended use is not permitted by statutory regulation or exceeds the permitted use, you will need to obtain permission directly from the copyright holder. To view a copy of this licence, visit http://creativecommons.org/licenses/by/4.0/.

References

Agboola, O.P., and M. Tunay. 2023. Urban resilience in the digital age: The influence of information-communication technology for sustainability. *Journal of Cleaner Production* 428: Article 139304.

AghaKouchak, A., L.S. Huning, F. Chiang, M. Sadegh, F. Vahedifard, O. Mazdiyasni, H. Moftakhari, and I. Mallakpour. 2018. How do natural hazards cascade to cause disasters?. *Nature* 561(7724): 458–460.

Alam, A., P. Sammonds, and B. Ahmed. 2020. Cyclone risk assessment of the Cox's Bazar district and Rohingya refugee camps in southeast Bangladesh. *Science of the Total Environment* 704: Article 135360.

Amirzadeh, M., S. Sobhaninia, and A. Sharifi. 2022. Urban resilience: A vague or an evolutionary concept?. *Sustainable Cities and Society* 81: Article 103853.

Bevacqua, E., M.I. Vousdoukas, G. Zappa, K. Hodges, T.G. Shepherd, D. Maraun, L. Mentaschi, and L. Feyen. 2020. More meteorological events that drive compound coastal flooding are projected under climate change. *Communications Earth & Environment* 1: 1–11.

Bristow, G., and A. Healy. 2018. Innovation and regional economic resilience: An exploratory analysis. *The Annals of Regional Science* 60(2): 265–284.

Chatti, W., and M.T. Majeed. 2022. Information communication technology (ICT), smart urbanization, and environmental quality: Evidence from a panel of developing and developed economies. *Journal of Cleaner Production* 366: Article 132925.

Chen, A., Y. Pokhrel, D. Chen, H. Huang, Z. Dai, B. He, J. Wang, and J. Li et al. 2024. Impact of tropical cyclones and socioeconomic exposure on flood risk distribution in the Mekong Basin. *Communications Earth & Environment* 5: Article 704.

Davtalab, M., and S. Byčenkienė. 2026. Synergistic effects of spatial urban form on PM2.5 concentration and urban heat islands: A multi-scale explanatory machine learning. *Journal of Cleaner Production* 538: Article 147226.

Folke, C. 2006. Resilience: The emergence of a perspective for social-ecological systems analyses. *Global Environmental Change* 16(3): 253–267.

Gori, A., N. Lin, D. Xi, and K. Emanuel. 2022. Tropical cyclone climatology change greatly exacerbates US extreme rainfall-surge hazard. *Nature Climate Change* 12: 171–178.

Huang, M., Q. Wang, M. Liu, N. Lin, Y. Wang, R. Jing, J. Sun, and H. Murakami et al. 2022. Increasing typhoon impact and economic losses due to anthropogenic warming in Southeast China. *Scientific Reports* 12: Article 14048.

Knutson, T.R., J.L. McBride, J. Chan, K. Emanuel, G. Holland, C. Landsea, I. Held, and J.P. Kossin et al. 2010. Tropical cyclones and climate change. *Nature Geoscience* 3: 157–163.

Kou, R., R. Hunter, C. Cleland, S. Ferguson, J. Schipperijn, Q. Peng, and G. Ellis. 2025. Built environment influences on park visits for older adults: Insights from a machine learning approach. *Cities* 165: Article 106143.

Laurien, F., S. Hochrainer-Stigler, A. Keating, K. Campbell, R. Mechler, and J. Czajkowski. 2020. A typology of community flood resilience. *Regional Environmental Change* 20: Article 24.

Li, Y., and L. Qiu. 2015. A comparative study on the quality of China's eco-city: Suzhou vs Kitakyushu. *Habitat International* 50: 57–64.

Li, J., J. Hu, Y. Yao, and N. Ren. 2025. Copula-based joint assessment of the extreme precipitation and storm surge along the coast of mainland China: Impact of tropical cyclones. *Journal of Hydrology* 662: Article 134124.

Liang, Y., C. Wang, G. Chen, and Z. Xie. 2024. Evaluation framework ACR-UFDR for urban form disaster resilience under rainstorm and flood scenarios: A case study in Nanjing. *China. Sustainable Cities and Society* 107: Article 105424.

Lin, J., P. He, L. Yang, X. He, S. Lu, and D. Liu. 2022. Predicting future urban waterlogging-prone areas by coupling the maximum entropy and FLUS model. *Sustainable Cities and Society* 80: Article 103812.

Lin, Y., C. Peng, J. Shu, W. Zhai, and J. Cheng. 2022. Spatiotemporal characteristics and influencing factors of urban resilience efficiency in the Yangtze River Economic Belt. *China. Environmental Science and Pollution Research* 29(26): 39807–39826.

Liu, D., J. Feng, H. Li, Q. Fu, M. Li, M.A. Faiz, S. Ali, and T. Li et al. 2019. Spatiotemporal variation analysis of regional flood disaster resilience capability using an improved projection pursuit model based on the wind-driven optimization algorithm. *Journal of Cleaner Production* 241: Article 118406.

Liu, W., J. Zhou, X. Li, H. Zheng, and Y. Liu. 2024. Urban resilience assessment and its spatial correlation from the multidimensional perspective: A case study of four provinces in North-South Seismic Belt. *China. Sustainable Cities and Society* 101: Article 105109.

Mallick, S.K., P. Das, B. Maity, S. Rudra, M. Pramanik, B. Pradhan, and M. Sahana. 2021. Understanding future urban growth, urban resilience and sustainable development of small cities using prediction-adaptation-resilience (PAR) approach. *Sustainable Cities and Society* 74: Article 103196.

Massaro, E., R. Schifanella, M. Piccardo, L. Caporaso, H. Taubenbock, A. Cescatti, and G. Duveiller. 2023. Spatially-optimized urban greening for reduction of population exposure to land surface temperature extremes. *Nature Communications* 14: Article 2903.

Mohtat, N., and L. Khirfan. 2022. Distributive justice and urban form adaptation to flooding risks: Spatial analysis to identify Toronto's priority neighborhoods. *Frontiers in Sustainable Cities* 4: Article 919724.

Mu, X., C. Fang, and Z. Yang. 2022. Spatio-temporal evolution and dynamic simulation of the urban resilience of Beijing-Tianjin-Hebei urban agglomeration. *Journal of Geographical Sciences* 32(9): 1766–1790.

Pee, L.G., and S.L. Pan. 2022. Climate-intelligent cities and resilient urbanisation: Challenges and opportunities for information research. *International Journal of Information Management* 63: Article 102446.

Pesaresi, M., H. Guo, X. Blaes, and D. Ehrlich. 2013. A global settlement layer from optical HR/VHR RS data: Concept and first results. *IEEE Journal of Selected Topics in Applied Earth Observations and Remote Sensing* 6: 2102–2131.

Qin, X., Y. Wu, H. Huang, X. Yang, and L. Gao. 2025. Impact of impervious surface spatial morphologies on urban waterlogging: Insights from a cascade modeling chain at catchment scale. *Sustainable Cities and Society* 130: Article 106912.

Ranjan, R., and S. Karmakar. 2024. Compound hazard mapping for tropical cyclone-induced concurrent wind and rainfall extremes over India. *Npj Natural Hazards* 1: Article 15.

Ruan, J., Y. Chen, and Z. Yang. 2021. Assessment of temporal and spatial progress of urban resilience in Guangzhou under rainstorm scenarios. *International Journal of Disaster Risk Reduction* 66: Article 102578.

Shafiei-Dastjerdi, M., and A. Lak. 2023. Towards resilient place emphasizing urban form: An assessment framework in urban design. *Sustainable Cities and Society* 96: Article 104646.

Sun, Y., Y. Wang, X. Zhou, and W. Chen. 2023. Are shrinking populations stifling urban resilience? Evidence from 111 resource-based cities in China. *Cities* 141: Article 104458.

Tian, Z., Y. Zhang, K. Udo, and X. Lu. 2023. Regional economic losses of China's coastline due to typhoon-induced port disruptions. *Ocean & Coastal Management* 237: Article 106533.

Tiggeloven, T., H. Moel, H. Winsemius, D. Eilander, G. Erkens, E. Gebremedhin, A. Loaiza, and S. Kuzma et al. 2020. Global-scale benefit-cost analysis of coastal flood adaptation to different flood risk drivers using structural measures. *Natural Hazards and Earth System Sciences* 20(4): 1025–1044.

UNISDR (United Nations International Strategy for Disaster Reduction). 2009. *Terminology on disaster risk reduction*. Geneva: UNISDR.

Wang, W., D. Kim, G. Kin, K.T. Kim, S. Kim, and H. Kim. 2024. Flood risk assessment of the Naeseongcheon Stream Basin, Korea using the grid-based flood risk index. *Journal of Hydrology: Regional Studies* 51: Article 101619.

Wu, N., Y. Zhou, S. Yin, H. Gong, and C. Zhang. 2025. Revealing the nonlinear impact of environmental regulation on ecological resilience using the XGBoost-SHAP model: Evidence from the Yangtze River Delta region. *China. Journal of Cleaner Production* 514: Article 145700.

Xi, L., Z. Qi, Y. Feng, X. Cao, J. Zou, and J. Han. 2026. An explainable machine learning approach (SHAP) to assessing desertification risk and its drivers in the Ring-Tarim Basin, 1990–2020. *Environmental Impact Assessment Review* 118: Article 108309.

Xie, W., C. Sun, and Z. Lin. 2023. Spatial-temporal evolution of urban form resilience to climate disturbance in adaptive cycle: A case study of Changchun City. *Urban Climate* 49: Article 101461.

Yang, X., Y. Yan, L. Zhou, M. Ma, J. Zhang, Y. Chen, and L. Gao. 2025. Risk of compound typhoon disaster chains: Insights from Southeastern China. *International Journal of Disaster Risk Science* 16(5): 870–887.

Yin, S., S. Rourou, W. Nannan, and Y. Jun. 2025. Measuring the impact of technological innovation on urban resilience through explainable machine learning: A case study of the Yangtze River Delta region. *China. Sustainable Cities and Society* 127: Article 106457.

Yu, S., X. Kong, Q. Wang, Z. Yang, and J. Peng. 2023. A new approach of robustness-resistance-recovery (3Rs) to assessing flood resilience: A case study in Dongting Lake Basin. *Landscape and Urban Planning* 230: Article 104605.

Zhang, T., Y. Sun, L. Yin, Y. Tian, Y. Sun, and B. Zhuang. 2025. Examining heat risk inequality from the perspective of urban resilience. *Sustainable Cities and Society* 131: Article 106743.

Zhu, S., D. Li, G. Huang, G. Chhipi-Shrestha, K.M. Nahiduzzaman, K. Hewage, and R. Sadiq. 2021. Enhancing urban flood resilience: A holistic framework incorporating historic worst flood to Yangtze River Delta, China. *International Journal of Disaster Risk Reduction* 61: Article 102355.

Zscheischler, J., S. Westra, B.J.J.M. van den Hurk, S.I. Seneviratne, P.J. Ward, A. Pitman, A. AghaKouchak, and D.N. Bresch et al. 2018. Future climate risk from compound events. *Nature Climate Change* 8: 469–477.

Zyl, C.V., X. Ye, and R. Naidoo. 2024. Harnessing explainable artificial intelligence for feature selection in time series energy forecasting: A comparative analysis of GradCAM and SHAP. *Applied Energy* 353: Article 122079.